

Effect of nuclear reactions rates and core boundary mixing on the seismology of Red Clump stars

Anthony Noll¹, Sarbani Basu², and Saskia Hekker^{1,3}

¹ Heidelberger Institut für Theoretische Studien, Schloss-Wolfsbrunnenweg 35, 69118 Heidelberg, Germany

² Department of Astronomy, Yale University, PO Box 208101, New Haven, CT 06520-8101, USA

³ Center for Astronomy (ZAH/LSW), Heidelberg University, Königstuhl 12, 69117 Heidelberg, Germany

January 12, 2024

ABSTRACT

Context. Modeling of the stars in the red clump (RC), i.e. core helium burning stars that have gone through a He-flash, is challenging, due to the uncertainties associated with the physical processes happening in their core and during the helium flash. By probing the internal stellar structure, asteroseismology allows us to constrain the core properties of RC stars and eventually improve our understanding of this evolutionary phase.

Aims. We aim to quantify the impact on the seismic properties of the RC stars of the two main core modeling uncertainties: core boundary mixing, and helium burning nuclear reaction rates.

Methods. Using the MESA stellar evolution code, we compute models with different core boundary mixing as well as different 3α and $^{12}\text{C}(\alpha, \gamma)^{16}\text{O}$ nuclear reaction rates. We investigate the impact of those parameters on the period spacing $\Delta\Pi$, which is a probe of the region around the core.

Results. We find that different core boundary mixing schemes yield significantly different period spacings, with differences of 30 s between the maximal $\Delta\Pi$ value computed with semiconvection and maximal overshoot. We show that increasing the rate of $^{12}\text{C}(\alpha, \gamma)^{16}\text{O}$ lengthens the core helium burning phase, which extends the range of $\Delta\Pi$ covered by the models during their evolution. This results in a difference of 10 s between the models computed with a nominal rate and a rate multiplied by 2, which is larger than the observational uncertainties. The effect of changing the 3α reaction rate is comparatively small.

Conclusions. The core boundary mixing is the main source of uncertainty regarding the seismic modeling of RC stars. Moreover, the effect of the $^{12}\text{C}(\alpha, \gamma)^{16}\text{O}$ is non-negligible, even if difficult to disentangle from the effect of the mixing. Such degeneracy could be raised in the future, thanks to new seismic data from the PLATO mission and theoretical constraints from numerical simulations.

1. Introduction

Stars in the red clump (RC) are somewhat high-metallicity (higher than approximately -0.6 dex), low-mass ($\lesssim 1.8 M_{\odot}$) stars that are in the process of fusing helium in their cores. Their key properties derive from the fact that their progenitors had a core made of degenerate matter when they were in the red giant branch (RGB) phase; this property results in helium core masses that are largely independent of the total mass. Consequently, properties of the RC stars have little dependency on the stellar mass, which makes them targets of significant astrophysical importance. RC stars have been proposed as standard candles (thanks to their narrow range of luminosity) and reddening indicators (Cannon 1970), as well as tracers of the chemical evolution of the Galaxy (e.g., Nidever et al. 2014). Since these stars are also the progenitors of later stages of stellar evolutions, improving their models is key to putting better constraints on the structure of, for instance, white dwarf stars.

However, the modeling of several physical processes occurring within RC stars is still uncertain. The first main unknown is mixing at the boundary of the convective core, which we refer to as core boundary mixing (CBM). Schwarzschild & Härm (1969) found the presence of a semiconvective region around the core, whose properties have been studied by Castellani et al. (1971b,a). However, the need for semiconvection was questioned by Bressan et al. (1986), who showed that including a strong overshoot (over a distance of the order of a pressure scale height) allows reproducing the star counts of globular clusters with no semiconvective region.

Other uncertainties in the modeling of RC stars are nuclear reactions rates, specifically the rates of the helium-burning 3α and $^{12}\text{C}(\alpha, \gamma)^{16}\text{O}$ reactions. The rate of the first reaction is somewhat well determined. However, the rate of the latter is notoriously ill-defined experimentally because the rates need to be extrapolated to low-energy stellar regimes, which is made more difficult by the presence of several interfering resonant states (Angulo et al. 1999; Kunz et al. 2002; deBoer et al. 2017).

Thanks to data from the space missions of the last decade, and especially *Kepler* (Borucki et al. 2010), it has been possible to retrieve the seismic properties of thousands of RC stars. RC stars are solar-like oscillators, with their modes being stochastically excited by the turbulence in the outer convective envelope of these stars. Notably, their non-radial modes have a mixed nature, acting as gravity modes in the core and pressure modes in layers above. Therefore, the study of these modes allows us to constrain the properties of the deep layers of the star, and especially probe the CBM. A striking result from the *Kepler* asteroseismic observables is that a large core extension is required to reproduce the observed seismic properties (e.g., Montalbán et al. 2013; Constantino et al. 2015; Bossini et al. 2015).

In this paper, we build on the works of Constantino et al. (2015, 2017) and Bossini et al. (2015, 2017) to investigate the combined effects of core boundary mixing, nuclear reactions rates and composition on the period spacing of RC stars. We probe a wide parameter space in order to assess the changes in the period spacings. We review, in Sect. 2 the seismic properties of RC stars and what structural features the period spacing

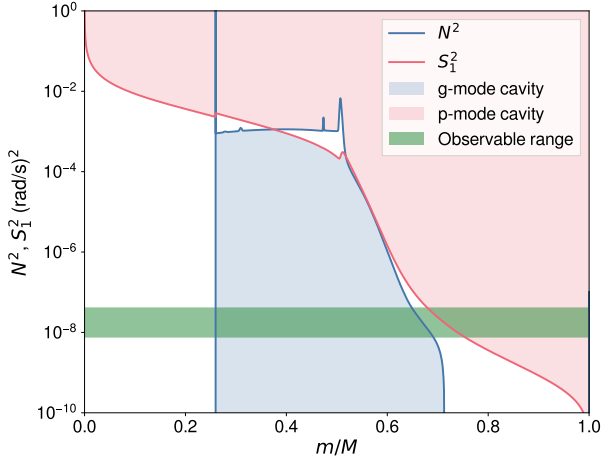


Fig. 1. Propagation diagram of an RC star. The Brunt-Väisälä frequency and $\ell = 1$ Lamb frequencies are shown with blue and pink lines, respectively. They delimit the g-mode (light blue) and p-mode (light pink) cavities. Finally, the typical range of observed frequencies is shown in green.

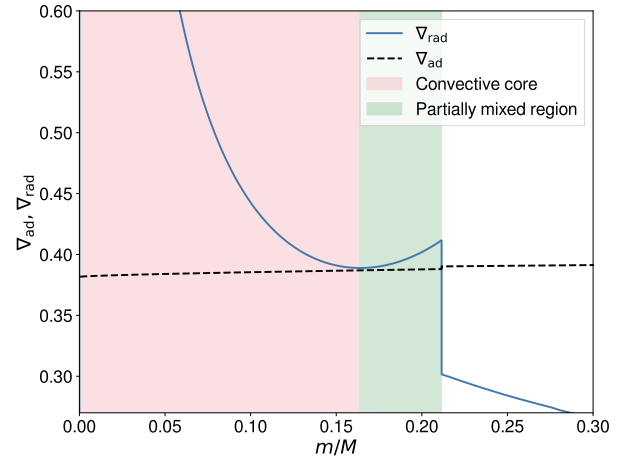


Fig. 2. Central structure of a $1 M_{\odot}$ core helium burning star in terms of radiative and adiabatic temperature gradients vs. the fractional mass. The radiative and adiabatic gradients are shown in solid blue and dashed black lines, respectively. We also show the convective core and partially mixed regions in pale pink and green.

probe. In Sect. 3, after describing the physics of the models, we explain the properties of the different CBM schemes used and their effect on the period spacing. In Sect. 4, we study the effect of varying the rates of $^{12}\text{C}(\alpha, \gamma)^{16}\text{O}$ and 3α on the period spacing. In Sect. 5, we look at the effect of the metallicity on the period spacing. Then, in Sect. 6, we look at the combined effects of CBM, nuclear reaction rates, and metallicity. We end with a discussion and a conclusion in Sect. 7 and 8, respectively.

2. Seismic properties of RC stars

Non-radial modes of RC stars are mixed modes, which behave like gravity modes in the g-mode cavity and like pressure modes in the p-mode cavity. For a mode whose angular frequency is ω , the g-mode cavity is delimited by $\omega^2 < N^2, S_{\ell}^2$, N being the Brunt-Väisälä frequency and S_{ℓ} the Lamb frequency for a mode with degree ℓ . Conversely, the p-mode cavity is defined by $\omega^2 > S_{\ell}^2, N^2$. In Fig. 1, we show those two cavities in an RC star. The g-mode cavity is located in the radiative region between the convective core and convective envelope, while the p-mode cavity is located in the outer layers of the star. The g-modes are therefore more sensitive to the inner part of the star, while the p-modes rather probe the envelope properties.

Pure g-modes are, asymptotically, equally spaced in period (Shibahashi 1979). The periods of consecutive modes of degree ℓ are separated by a period spacing $\Delta\Pi_{\ell}$, which is defined as:

$$\Delta\Pi_{\ell} = \frac{2\pi^2}{\sqrt{\ell(\ell+1)}} \left(\int_{r_0}^{r_1} \frac{N}{r} dr \right)^{-1}, \quad (1)$$

where r is the radial coordinate and r_0, r_1 are the limits of the g-mode cavity. In the following, we only look at the period spacing of dipole modes, since we only observe those modes; for simplicity we call this $\Delta\Pi$. Through the integral of N/r in the g-mode cavity, $\Delta\Pi$ is tightly related to the size of the convective core. Indeed, a larger convective core would make the g-mode cavity smaller and accordingly increase $\Delta\Pi$, making the period spacing a very good probe of the properties near the convective core and a precise measure of the mass of the helium core (Montalbán et al. 2013). In this paper, we compute $\Delta\Pi$ using Eq. (1).

It will be the main seismic observable of interest, as we study the effect of helium burning reactions which happen in the core of the star.

Thanks to the *Kepler* satellite data, period spacing can be measured for thousands of RC stars. It covers a range of period spacing from approximately 230 to 340 seconds, largely independently of the mass (Vrard et al. 2016), as we can expect from those low-mass stars which had a degenerate core on the red giant branch.

3. Physics of the models

3.1. General properties

We computed models with MESA version r22.11.1 (Paxton et al. 2011, 2013, 2015, 2018, 2019; Jermyn et al. 2023). The equation of state is a mix of FreeEOS (Irwin 2012) in the envelope and Skye (Jermyn et al. 2021) in the core. The opacities come from the OPAL code (Iglesias & Rogers 1996), and we use the solar mixture of Grevesse & Sauval (1998). The convection regions are computed using the time-dependent local Kuhfuss (1986) model, adapted in such a way that it reduces to Cox & Giuli (1968) mixing-length prescription at typical stellar evolutionary times. We set the mixing-length parameter α_{MLT} to 1.8. The nuclear reaction rates are from the REA CLIB database¹ (Cyburt et al. 2010). Any modification in the nuclear reaction rates described in the text are with respect to these rates.

3.2. Core boundary mixing

During the helium-burning phase, the core becomes enriched in carbon and oxygen, which increases the opacity and thus the radiative gradient, leading to a growing core. Once the core reaches a certain size, the radiative gradient within it is not monotonic

¹ During this work, it has been found that the above version of MESA has a faulty implementation of the reverse 3α reaction, which causes a depletion of carbon at the end of the core helium-burning phase. However, it does not affect us since we do not take this reaction into account in our nuclear network because its rate is extremely low at temperatures relevant to our study. We are therefore not concerned by this issue.

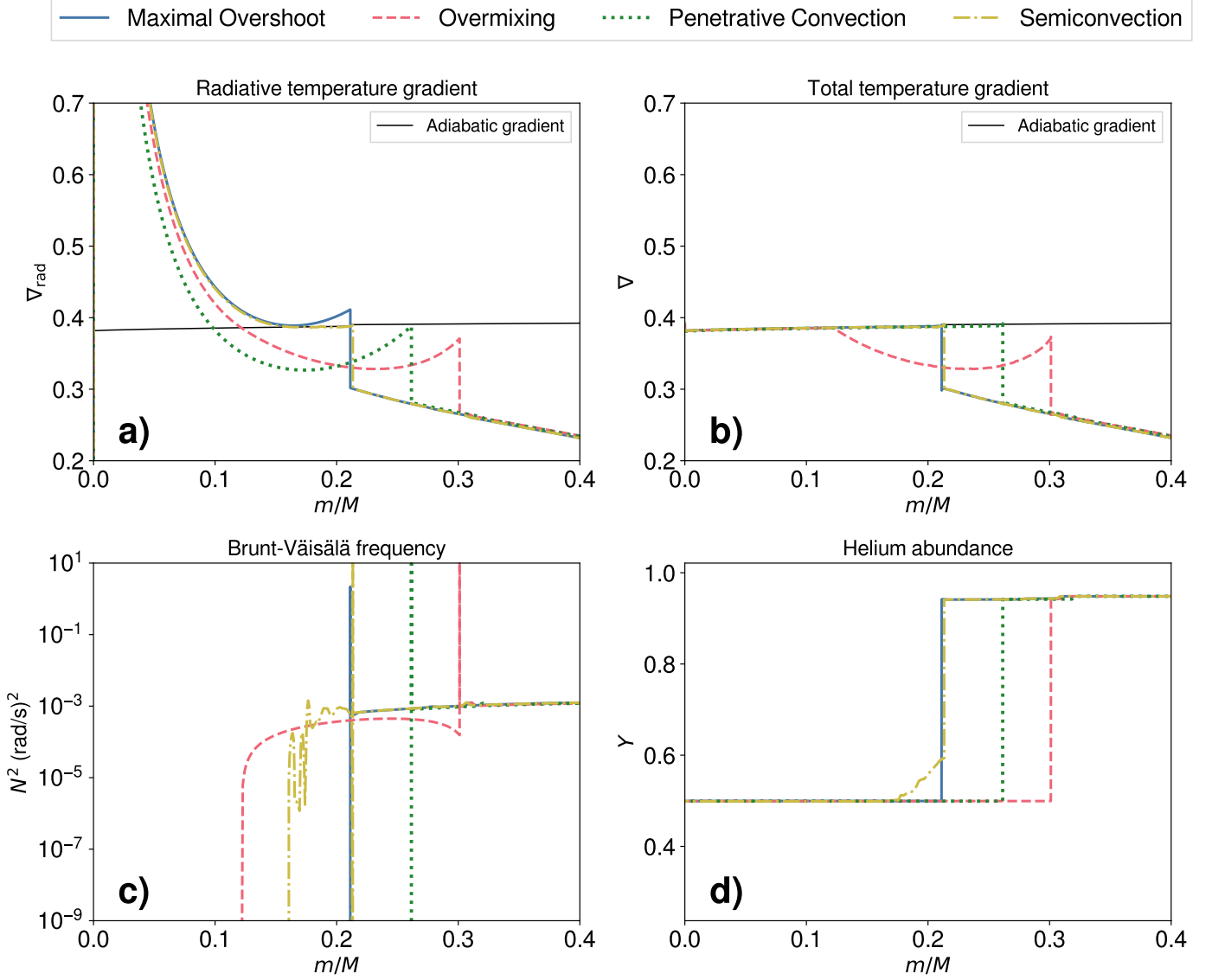


Fig. 3. Properties around the core of $1 M_{\odot}$, solar-metallicity models computed with the Maximal overshoot (blue, solid), overmixing (pink, dashed), penetrative convection (green, dotted) and semiconvection (yellow, dash-dotted) core boundary mixing schemes. *Panel a:* Radiative and adiabatic gradients. *Panel b:* Temperature gradients ($\nabla = \partial \ln T / \partial \ln P$). *Panel c:* Brunt-Väisälä frequency profile. *Panel d:* Helium composition profile.

anymore and, after a minimum, increases with radius. Such a radiative temperature gradient is illustrated in Fig. 2. The core is then split in two regions: the fully mixed core (between the center and the minimum of ∇_{rad}) and the *partially mixed* (PM) region, between the minimum of ∇_{rad} and the radiative region. The properties of the PM region have a significant effect on the Brunt-Väisälä frequency profile, and therefore on the asymptotic period spacing. Thus, we examine the effect of different partial mixing prescriptions in this work. As an illustration, we show in Fig. 3 the profile of different properties (temperature gradients, Brunt-Väisälä frequency, and composition) for the four different mixing prescriptions, which we describe below.

Semiconvection: Schwarzschild & Härm (1969) found that the PM region is a *semiconvective* region, which is buoyantly neutral (i.e., $\nabla_{\text{rad}} = \nabla_{\text{ad}}$). To achieve that, we use in this work the convective premixing (CPM) scheme (Paxton et al. 2019). This scheme treats every convective boundary with an iterative approach (within an evolutionary timestep) such that the

Schwarzschild (or Ledoux) criterion is respected on the convective side of the boundary (in accordance with the recommendation from Gabriel et al. 2014). To explain how the CPM scheme leads to the formation of a semiconvective region, let us start from a situation similar to the one shown in Fig. 2. One can see that, at the outer boundary of the partially PM region, $\nabla_{\text{rad}} > \nabla_{\text{ad}}$ which causes the boundary to move to a larger radius due to overshooting. This brings fresh unburned helium in the PM region that lowers the opacity in the PM region and therefore the radiative gradient. As a consequence, the inner PM region boundary, which was defined by the local minimum of the radiative gradient and was marginally unstable, moves to a larger radius, leaving a buoyantly neutral region in its wake. This process repeats, until the full PM region is buoyantly neutral. This mechanism of mixing through successive shrinking convective shells has been described by Gabriel (1970) for massive star models, and is similar to the Castellani et al. (1985) semiconvection scheme for core helium burning (CHeB) stars.

Semiconvection is sensitive to the core breathing pulses (CBP), which occur at the end of the core-helium burning phase. These pulses are sudden increases of the core size that are caused by the strong increase of energy produced by the 3α triple alpha reaction when a small (in absolute sense) but high (in relative sense) quantity of helium is injected in the core. This unstable behavior impacts both $\Delta\Pi$ and the duration of the core-helium burning phase. However, CBP seem to be ruled out by observations of globular clusters and asteroseismology (Caputo et al. 1989; Cassisi et al. 2001; Constantino et al. 2017). For that reason, we avoid the increase of central helium abundance during the CHeB phase. This helps to reduce the number of CBP, without totally eliminating them. Finally, Constantino et al. (2015) observed that mode trapping may occur in the semiconvective region, which may impact the seismic properties of the star. We discuss this process in Sect. 7.1.

Maximal overshoot: This scheme was introduced by Constantino et al. (2015) to reconcile model predictions with seismic observations, and results in a large asymptotic period spacing. It is defined by the following algorithm: once the local ∇_{rad} minimum appears in the core, it extends the core such that the local minimum of the radiative gradient is equal to the adiabatic gradient. A core larger than this would decrease the radiative gradient, which would split the convective region in two and thus lower the period spacing. This scheme is ad-hoc and quite nonphysical, notably by the fact that the Schwarzschild criterion is not respected on the convective side of the external boundary (see Fig. 3 a). However, it leads to a behavior of the period spacing that is similar to the one resulting from a potential mode trapping in the semiconvective region, which we discuss in Sect. 7.1.

Overmixing and penetrative convection: The core can be extended over a certain distance d_{ov} , defined by a free parameter α_{ov} such that $d_{\text{ov}} = \alpha_{\text{ov}} H_p$, with H_p the pressure scale height. The thermal stratification in the extension region can either be radiative (i.e., $\nabla = \nabla_{\text{rad}}$) or adiabatic (i.e., $\nabla = \nabla_{\text{ad}}$). The first case is known as *overmixing* while the second is known as *penetrative convection*. We note that, at some point in the evolution, a convective shell appears at the outer boundary of the overshooting region. This shell becomes a semiconvective region, when using a convective premixing scheme. Note that the overmixing and penetrative convection schemes used here are different from the ones used in Bossini et al. (2015, 2017), due to the presence of this semiconvective region. More details on the effect of α_{ov} and the core boundary scheme are given in Sect. 7.2.

Fig. 4 shows the evolution of the asymptotic period spacing $\Delta\Pi$ of $1.0 M_{\odot}$ models with solar metallicity and different core boundary mixing prescriptions. We use $\alpha_{\text{ov}} = 1.0$ for overmixing and penetrative convection. As expected, every prescription yields significantly different ranges of $\Delta\Pi$. Notably, the maximum value of period spacing for models with semiconvection is approximately 290s, which is significantly lower than the highest observational values of Vrad et al. (2016). Both maximal overshoot and overmixing schemes show similar behavior, with a continuous growth of the core. Finally, the penetrative convection has a behavior similar to the overmixing scheme, but approximately 30 s higher.

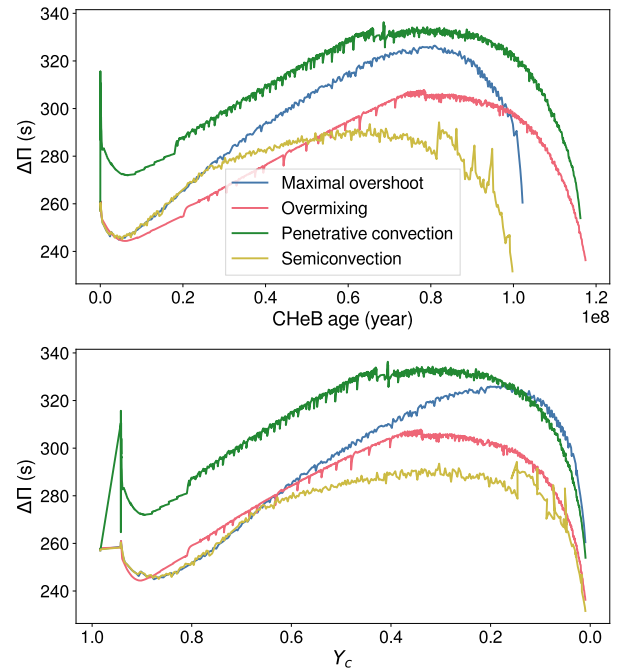


Fig. 4. Evolution of $\Delta\Pi$ of a $1 M_{\odot}$ model of solar metallicity for different core-boundary mixing prescriptions. The evolution is indicated with age (upper panel) and central helium abundance Y_c (lower panel).

Table 1. Nuclear rate of the $^{12}\text{C}(\alpha, \gamma)^{16}\text{O}$ reaction, at 10^8 K, from different literature sources.

Reference	Rate value ($\text{cm}^3 \text{s}^{-1} \text{mol}^{-1}$)
Angulo et al. (1999)	$1.81^{+0.74}_{-0.75} \times 10^{-20}$
Kunz et al. (2002)	$1.29^{+0.44}_{-0.39} \times 10^{-20}$
Xu et al. (2013)	$1.15^{+0.21}_{-0.20} \times 10^{-20}$
deBoer et al. (2017)	$1.20^{+0.20}_{-0.20} \times 10^{-20}$
Shen et al. (2023)	1.42×10^{-20}

4. Effect of nuclear reaction rates on the seismic observables

4.1. Nuclear reactions in RC stars

Helium burning mainly happens through two reactions. The first is the 3α process, which occurs in two steps: $^4\text{He} + ^4\text{He} \rightarrow ^7\text{Be}$ and $^7\text{Be} + ^4\text{He} \rightarrow ^{12}\text{C} + \gamma$. This reaction dominates during the early part of the helium burning phase. The second reaction is the $^{12}\text{C}(\alpha, \gamma)^{16}\text{O}$ reaction ($^{12}\text{C} + ^4\text{He} \rightarrow ^{16}\text{O} + \gamma$) which dominates at the end of the helium burning phase.

The formal uncertainties on the 3α reaction are relatively low, being of the order of 10% in the NACRE compilation (Angulo et al. 1999). For the $^{12}\text{C}(\alpha, \gamma)^{16}\text{O}$ reaction, Table 1 summarizes the rate at 0.1 GK found in the literature. Notably, the work by Kunz et al. (2002) considerably lowered the nominal rate compared to the NACRE compilation. One can also note the recent results of Shen et al. (2023), who found a rate significantly higher than the values of Xu et al. (2013) and deBoer et al. (2017). The value of the $^{12}\text{C}(\alpha, \gamma)^{16}\text{O}$ rate is, therefore, still uncertain.

In this work, the standard rate for the 3α and $^{12}\text{C}(\alpha, \gamma)^{16}\text{O}$ reactions are assumed to be the rates from Fynbo et al. (2005) and Xu et al. (2013), respectively. The models described in this

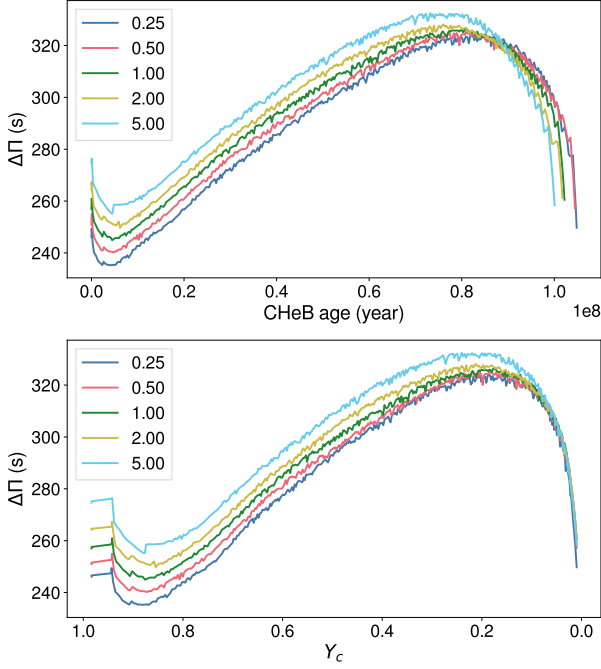


Fig. 5. Evolution of $\Delta\Pi$ during the CHeB phase, for different 3α reaction rates.

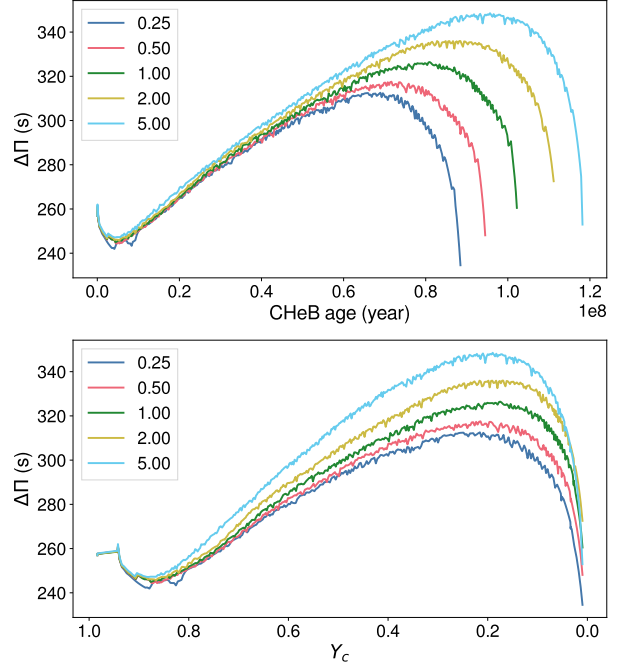


Fig. 6. Same as Fig. 5, now for different $^{12}\text{C}(\alpha, \gamma)^{16}\text{O}$ reaction rates.

section are $1 M_{\odot}$ models with solar metallicity, and computed with the maximal overshoot scheme.

4.2. Effect of the nuclear reactions rates on the period spacing

4.2.1. 3α Reaction

In Fig. 5 we show the evolution of $\Delta\Pi$ during the core-helium burning phase for different factors by which the standard 3α reaction rate was changed. One can see that increasing the rate of the 3α process yields models with higher asymptotic period spacing during the whole helium burning phase. For instance, multiplying the rate by 2 increases the period spacing by approximately 4 s, which is consistent with the results of Constantino et al. (2015).

This effect on the period spacing is due to two competing processes: 1) Higher 3α rate allows the He-flash to start at lower temperature, i.e., earlier in the RGB evolution. The inert He-core is therefore less massive, and so is the convective core during the CHeB phase. This decreases the asymptotic period spacing. 2) Because of the higher rate, the same luminosity can be produced in a lower density environment. This lowers the local gravity within the star and thus the Brunt-Väisälä frequency, eventually yielding a higher period spacing. The amplitude of the second process is slightly larger than the first one, which explains the fact that period spacing is higher with an increase 3α rate.

4.2.2. $^{12}\text{C}(\alpha, \gamma)^{16}\text{O}$ Reaction

In Fig. 6 we show the evolution of $\Delta\Pi$ for different rates of the $^{12}\text{C}(\alpha, \gamma)^{16}\text{O}$ reaction. We find that at first, for a CHeB age below 0.4×10^8 years, the period spacings of the different models are identical. This is because initially the $^{12}\text{C}(\alpha, \gamma)^{16}\text{O}$ produces a negligible part of the total luminosity of the star. The main effect of increasing the rate of $\Delta\Pi$ is to extend the CHeB phase. Indeed,

models with a rate that is multiplied by 5 have a CHeB duration approximately 20% longer.

The core expands during core helium burning, which increases continuously the period spacing. Therefore, by extending the CHeB phase, the models reach higher $\Delta\Pi$ values. Thus, models with a rate multiplied by 2 cover a period spacing range of 89 s, that is 10 s larger than the models with a standard rate. We note that Constantino et al. (2015) found the same order of magnitude, but surprisingly did not find that increasing the $^{12}\text{C}(\alpha, \gamma)^{16}\text{O}$ rate lengthens the CHeB phase, contrary to results presented in earlier literature (e.g., Salaris & Cassisi 2005).

To explain the increase of the duration of the CHeB phase, we show in Fig. 7 the share of the luminosity production between the different reactions, for a model with a standard rate (left) and with a rate multiplied by 5 (right). The total luminosities of the two models are very similar, but the distribution of energy production between the reactions differ. Indeed, at a given Y_c , $^{12}\text{C}(\alpha, \gamma)^{16}\text{O}$ produces a more significant fraction of the energy when its rate is multiplied by 5. Yet, one $^{12}\text{C}(\alpha, \gamma)^{16}\text{O}$ reaction consumes one nucleus of helium while the 3α reaction consumes three, for an approximately equal amount of energy production. Consequently, the helium consumption will be lowered if $^{12}\text{C}(\alpha, \gamma)^{16}\text{O}$ dominates at a given total luminosity. This results in an increase of the duration of the core-helium burning phase, which in turn increases the range of $\Delta\Pi$ during the CHeB phase. We note that similar results and explanations have recently been found by Tognini et al. (2023).

5. Effect of composition

Metallicity has a significant impact on the period spacing during the CHeB phase. Indeed, a metal-poor star ignites helium at a more massive core, which in turn affects the size of the convective helium-burning core (see e.g., Sweigart & Gross 1976). Consequently, we expect a higher period spacing for metal-poor models, which is verified in our models, as shown in Fig. 8. In addition, decreasing the metallicity shortens the CHeB dura-

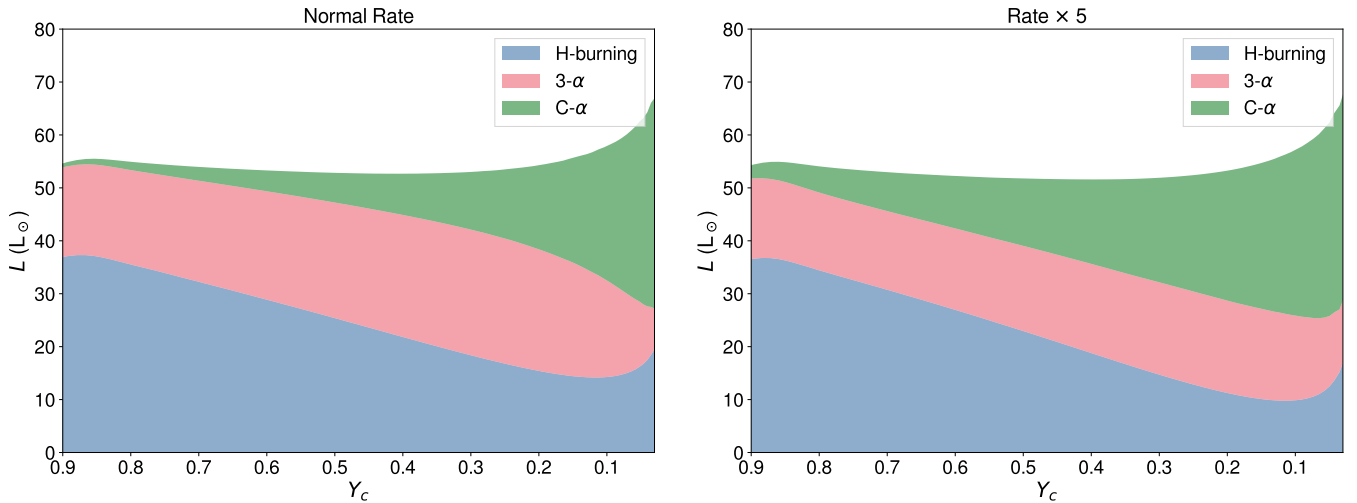


Fig. 7. Evolution of the distribution of the total luminosity of a $1 M_{\odot}$ CHEB star between the different nuclear reactions, for a star with a normal rate and a rate multiplied by 5.

tion. Figure 8 shows the evolution of the period spacing for $1 M_{\odot}$ models, computed with a maximal overshoot scheme at different metallicities. We found that stars with a metallicity of 0.2 dex have a period spacing roughly 25 s lower than a model with a metallicity of -0.5 dex, during the whole CHEB phase. These results are consistent with the findings of Constantino et al. (2017) and Bossini et al. (2017).

In contrast with the metallicity, the models show that the initial helium Y_0 has a small impact on the period spacing, except at the very beginning of the core helium burning phase. In Fig. 8, we illustrate this with a model computed with 0.2 dex metallicity and $Y_0 = 0.25$, rather than the original $Y_0 = 0.29$ metallicity.

6. Combined effect of mixing, nuclear reaction rates and metallicity

In this section, we look at the combined effect of the core boundary mixing, nuclear reaction rates of $^{12}\text{C}(\alpha, \gamma)^{16}\text{O}$ and metallicity on the period spacing. Figure 9 shows the span of period spacing for models with different mixing, metallicities and $^{12}\text{C}(\alpha, \gamma)^{16}\text{O}$ nuclear reaction rates. We choose metallicity values of -0.5 and 0.2 dex, which encompass the metallicities of the stars in the *Kepler* field. The values for the rates are half, double, and equal to the standard rate.

From this figure, we find that, on the one hand, the penetrative convection scenario, when computed with $\alpha_{\text{ov}} = 1.0$, can reproduce the highest observed values of period spacing, but not the lowest. On the other hand, the models computed with penetrative convection and $\alpha_{\text{ov}} = 0.1$ can reproduce the lower values but not the higher values. Thus, no value of α_{ov} seems to allow the penetrative convection to be compatible with the observations.

The asymptotic period spacing of the models computed with semiconvection and overmixing (for both $\alpha_{\text{ov}} = 1.0$ and 0.1) cannot reproduce the full range of observed values, especially the highest values. However, maximal overshoot yields scenarios which are compatible with the observations.

We note that the effect of increasing the rate is higher for models computed with maximal overshoot (increase of the maximal value of period spacing of 10 s) compared to models computed with a semiconvective region (increase of 7 s). This effect

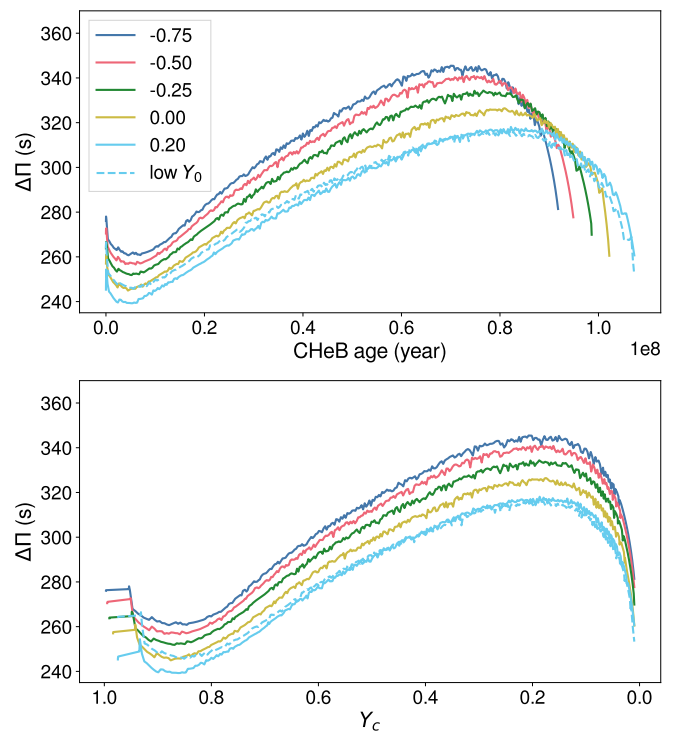


Fig. 8. Evolution of $\Delta\Pi$ for different metallicities, at $1.0 M_{\odot}$. A model with $Y_0 = 0.25$ and high metallicity is also shown.

does also depend, but only slightly, on the metallicity, with a stronger effect for models with lower metallicity (the increase is 2 s larger for -0.5 dex).

Finally, it seems difficult to disentangle the different reaction rates, due to the uncertainties on the core boundary mixing and the rather strong effect of metallicity.

7. Discussion

7.1. Mode trapping

In models with overmixing or semiconvection, the PM region is part of the g-mode cavity and its outer boundary is delimited by a strong chemical discontinuity. For those reasons, as noted by Constantino et al. (2015), some modes may be trapped within the PM region while the other modes are trapped in the rest of the g-mode cavity. Consequently, their frequencies behave as if the inner boundary of their cavity is the outer boundary of the PM region. For this reason, the observed period spacing, obtained with frequencies, may be significantly higher than the asymptotic period spacing as defined in Eq. 1 (Constantino et al. 2015; Pinçon & Takata 2022).

We did not explicitly account for this process in our work. However, the period spacing yielded by the maximal overshoot scheme is close to the observed period spacing that would result from mode trapping in a semiconvective region. This is due to the fact that the extent of the maximal overshoot core is close to the extent of the core plus the semiconvection region. We can therefore consider that the results coming from the maximal overshoot scheme are, at least for $\Delta\Pi$, equivalent to the trapped mode scenario in the case of semiconvection.

A thorough study of the mode trapping phenomenon in RC stars is beyond the scope of this paper. We note nevertheless that we observed such trapping in a subset of our models with semiconvection and overmixing when computing frequencies (with, e.g., GYRE Townsend & Teitler 2013). The development of trapped modes seems to depend, though, on the physics of the models, especially the inclusion of microscopic diffusion.

7.2. Effect of the core boundary scheme and α_{ov} in the overshoot models

In this section, we discuss the different ways to handle the boundary of the convective region with overshoot, as well as the effect of α_{ov} .

The burning of helium in the core increases the opacity, which in turn increases the radiative gradient. Thus, the local maximum of ∇_{rad} situated at the outer overshoot boundary (see panel a of Fig. 3) becomes at some point in the evolution larger than ∇_{ad} , which makes the outer part of the overshoot region convective. Such convective shell is stable if we use the basic convective boundary scheme, which can be questioned (see Sect. 7 of Gabriel et al. 2014). However, if we use the convective premixing scheme (CPM), as done in this work, the convective shell becomes semiconvective, which impacts the Brunt-Väisälä frequency profile and therefore the period spacing. Fig. 10 and 11 illustrates this effect for overmixing and penetrative convection, respectively. Notably, we can see that using the CPM lowers the period spacing once the semiconvective region appears. Consequently, our models have period spacings with maximal values that are lower than the ones computed without a semiconvective region, such as in Bossini et al. (2015, 2017).

Another effect of the CPM scheme is to make the evolution of the core boundary smoother at low overshoot. Indeed, as noted in Straniero et al. (2003), if a convective shell is present in the overshoot region, it intermittently merges with the convective core which suddenly expands it. Then, there is a strong helium intake and the core size reduces. Such erratic core behavior is visible in the evolution of the period spacing for models with

low overshoot², as we can see in Fig. 10 and 11, while the evolution of period spacing when computed with CPM appears to be smoother.

Regarding the effect of the α_{ov} parameter on the period spacing, it differs between the overmixing and penetrative convection cases. In the first case, it does not impact $\Delta\Pi$ much due to the fact that the overshoot region is part of the g-mode cavity, as one can see in panel c) of Fig. 3. Therefore, modifying the extent of the overshoot region does not directly impact the extent of the g-mode cavity, which limits the effect of the parameter on the period spacing. However, the smaller the α_{ov} the parameter the sooner the semiconvective region appears (as noted by the arrows), which decreases the maximum value of the period spacing as one can see in Fig. 10.

For the penetrative convection case, the g-modes do not propagate in the overshoot region. Thus, increasing α_{ov} increases the period spacing, as we can see in Fig. 11. Also, similarly to the models with overmixing, the semiconvection region appears sooner in the evolution for models with low α_{ov} . Due to these two effects, α_{ov} has a considerable effect on $\Delta\Pi$ for models with penetrative convection.

8. Conclusion

In this paper, we investigated the combined effects of the 3α and $^{12}\text{C}(\alpha, \gamma)^{16}\text{O}$ reaction rates, core boundary mixing and metallicity on the period spacing of RC stars. These stars exhibit mixed modes whose properties, and especially the period spacing $\Delta\Pi$, allow us to probe the properties of the region around the core. We found, in accordance with the literature (Constantino et al. 2015, 2017; Bossini et al. 2015, 2017), that the core boundary mixing scheme is the main source of uncertainties on the period spacing of our models, as the period spacing strongly depends on the size of the convective core, as well as on the temperature and composition stratification in the core boundary region. We confirm the findings of Constantino et al. (2015) that the maximal overshoot is the only scheme able to reproduce the lowest and highest values of $\Delta\Pi$. Additionally, we found that, even if the scheme itself is ad-hoc, the resulting period spacings are similar to those that result from mode trapping in a semiconvective region. We also tested overmixing ($\nabla = \nabla_{rad}$ in the overshoot region) and penetrative convection ($\nabla = \nabla_{ad}$ in the overshoot region). We found that, no single value of the overshoot parameter can reproduce both the highest and lowest observed values of $\Delta\Pi$. These results differ from those of Bossini et al. (2015, 2017). This difference is due to the use of the convective premixing scheme in this work, which causes a semiconvective region around the core which decreases the value of the period spacing. This semiconvection region notably solves the issue of an unphysical core boundary, in which $\nabla_{rad} > \nabla_{ad}$ at the inner side of the boundary.

We also investigated the effect of changing the rates of the 3α and $^{12}\text{C}(\alpha, \gamma)^{16}\text{O}$ reactions. On the one hand, regarding the 3α reaction, a higher rate causes an earlier helium flash and a lower central density during the helium-burning phase. These effects decrease and increase the period spacing, respectively, such that the resulting effect is negligible. On the other hand, the effect of increasing the rate of the $^{12}\text{C}(\alpha, \gamma)^{16}\text{O}$ reaction is, mainly, to increase the duration of the CHeB phase. This allows the cores to grow to a larger size, which eventually increases the maximum

² The reason such erratic evolution of $\Delta\Pi$ does not happen at high α_{ov} is due to the fact that, as the overshoot region is larger, the convective shell is more distant from the core and thus never merges.

value of the period spacing. We find that doubling the rate increases the maximum period spacing value by 10 s for a model computed with maximal overshoot, and 7 s for a model computed with the convective premixing scheme without overshoot. The effect of increasing the rate is slightly higher for models with lower metallicity, but with a negligible amplitude (2 s higher for a -0.5 dex model).

Mainly due to the uncertainties on the mixing³, it is for the moment not (yet) possible to perform an inverse analysis, i.e., constrain the $^{12}\text{C}(\alpha, \gamma)^{16}\text{O}$ rate using the period spacing of the RC stars. However, with better constraints on the core boundary mixing, as well as more data with the upcoming PLATO mission (Rauer et al. 2014), RC stars seismology could provide astrophysical constraints on the $^{12}\text{C}(\alpha, \gamma)^{16}\text{O}$ reaction rate.

Acknowledgements. We thank the anonymous referee for comments that improved the clarity of this paper. AN and SH acknowledge funding from the ERC Consolidator Grant DipolarSound (grant agreement #10s1000296). SB acknowledges NSF grant AST-2205026.

References

- Angulo, C., Arnould, M., Rayet, M., et al. 1999, Nucl. Phys. A, 656, 3
- Blouin, S., Herwig, F., Mao, H., Denissenkov, P., & Woodward, P. R. 2023, MNRAS[arXiv:2308.10865]
- Borucki, W. J., Koch, D., Basri, G., et al. 2010, Science, 327, 977
- Bossini, D., Miglio, A., Salaris, M., et al. 2015, MNRAS, 453, 2290
- Bossini, D., Miglio, A., Salaris, M., et al. 2017, MNRAS, 469, 4718
- Bressan, A., Bertelli, G., & Chiosi, C. 1986, Mem. Soc. Astron. Italiana, 57, 411
- Cannon, R. D. 1970, MNRAS, 150, 111
- Caputo, F., Castellani, V., Chieffi, A., Pulone, L., & Tornambe, A., J. 1989, ApJ, 340, 241
- Cassisi, S., Castellani, V., Degl’Innocenti, S., Piotto, G., & Salaris, M. 2001, A&A, 366, 578
- Castellani, V., Chieffi, A., Tornambe, A., & Pulone, L. 1985, ApJ, 296, 204
- Castellani, V., Giannone, P., & Renzini, A. 1971a, Ap&SS, 10, 355
- Castellani, V., Giannone, P., & Renzini, A. 1971b, Ap&SS, 10, 340
- Constantino, T., Campbell, S. W., Christensen-Dalsgaard, J., Lattanzio, J. C., & Stello, D. 2015, MNRAS, 452, 123
- Constantino, T., Campbell, S. W., & Lattanzio, J. C. 2017, MNRAS, 472, 4900
- Cox, J. P. & Giuli, R. T. 1968, Principles of stellar structure
- Cybur, R. H., Amthor, A. M., Ferguson, R., et al. 2010, ApJS, 189, 240
- deBoer, R. J., G rres, J., Wiescher, M., et al. 2017, Reviews of Modern Physics, 89, 035007
- Fynbo, H. O. U., Diget, C. A., Bergmann, U. C., et al. 2005, Nature, 433, 136
- Gabriel, M. 1970, A&A, 6, 124
- Gabriel, M., Noels, A., Montalb n, J., & Miglio, A. 2014, A&A, 569, A63
- Grevesse, N. & Sauval, A. J. 1998, Space Sci. Rev., 85, 161
- Iglesias, C. A. & Rogers, F. J. 1996, ApJ, 464, 943
- Irwin, A. W. 2012, FreeEOS: Equation of State for stellar interiors calculations, Astrophysics Source Code Library, record ascl:1211.002
- Jermyn, A. S., Bauer, E. B., Schwab, J., et al. 2023, ApJS, 265, 15
- Jermyn, A. S., Schwab, J., Bauer, E., Timmes, F. X., & Potekhin, A. Y. 2021, ApJ, 913, 72
- Kuhfuss, R. 1986, A&A, 160, 116
- Kunz, R., Fey, M., Jaeger, M., et al. 2002, ApJ, 567, 643
- Montalb n, J., Miglio, A., Noels, A., et al. 2013, ApJ, 766, 118
- Nidever, D. L., Bovy, J., Bird, J. C., et al. 2014, ApJ, 796, 38
- Paxton, B., Bildsten, L., Dotter, A., et al. 2011, ApJS, 192, 3
- Paxton, B., Cantiello, M., Arras, P., et al. 2013, ApJS, 208, 4
- Paxton, B., Marchant, P., Schwab, J., et al. 2015, ApJS, 220, 15
- Paxton, B., Schwab, J., Bauer, E. B., et al. 2018, ApJS, 234, 34
- Paxton, B., Smolec, R., Schwab, J., et al. 2019, ApJS, 243, 10
- Pin on, C. & Takata, M. 2022, A&A, 661, A139
- Rauer, H., Catala, C., Aerts, C., et al. 2014, Experimental Astronomy, 38, 249
- Salaris, M. & Cassisi, S. 2005, Evolution of Stars and Stellar Populations, 162–163
- Schwarzschild, M. & H rm, R. 1969, in BAAS, Vol. 1, 99
- Shen, Y., Guo, B., deBoer, R. J., et al. 2023, ApJ, 945, 41
- Shibahashi, H. 1979, PASJ, 31, 87
- Straniero, O., Dom nguez, I., Imbriani, G., & Piersanti, L. 2003, ApJ, 583, 878
- Sweigart, A. V. & Gross, P. G. 1976, ApJS, 32, 367
- Tognini, F., Valle, G., Dell’Omodarme, M., Degl’Innocenti, S., & Prada Moroni, P. G. 2023, A&A, 679, A75
- Townsend, R. H. D. & Teitler, S. A. 2013, MNRAS, 435, 3406
- Vrard, M., Mosser, B., & Samadi, R. 2016, A&A, 588, A87
- Xu, Y., Takahashi, K., Goriely, S., et al. 2013, Nucl. Phys. A, 918, 61

³ We note the recent work from Blouin et al. (2023), which through 3D simulations, explore the stability of the different core boundary mixing schemes used in this work, and find that a semiconvective region is quickly erased by overshooting mixing through overshooting from the convective core.

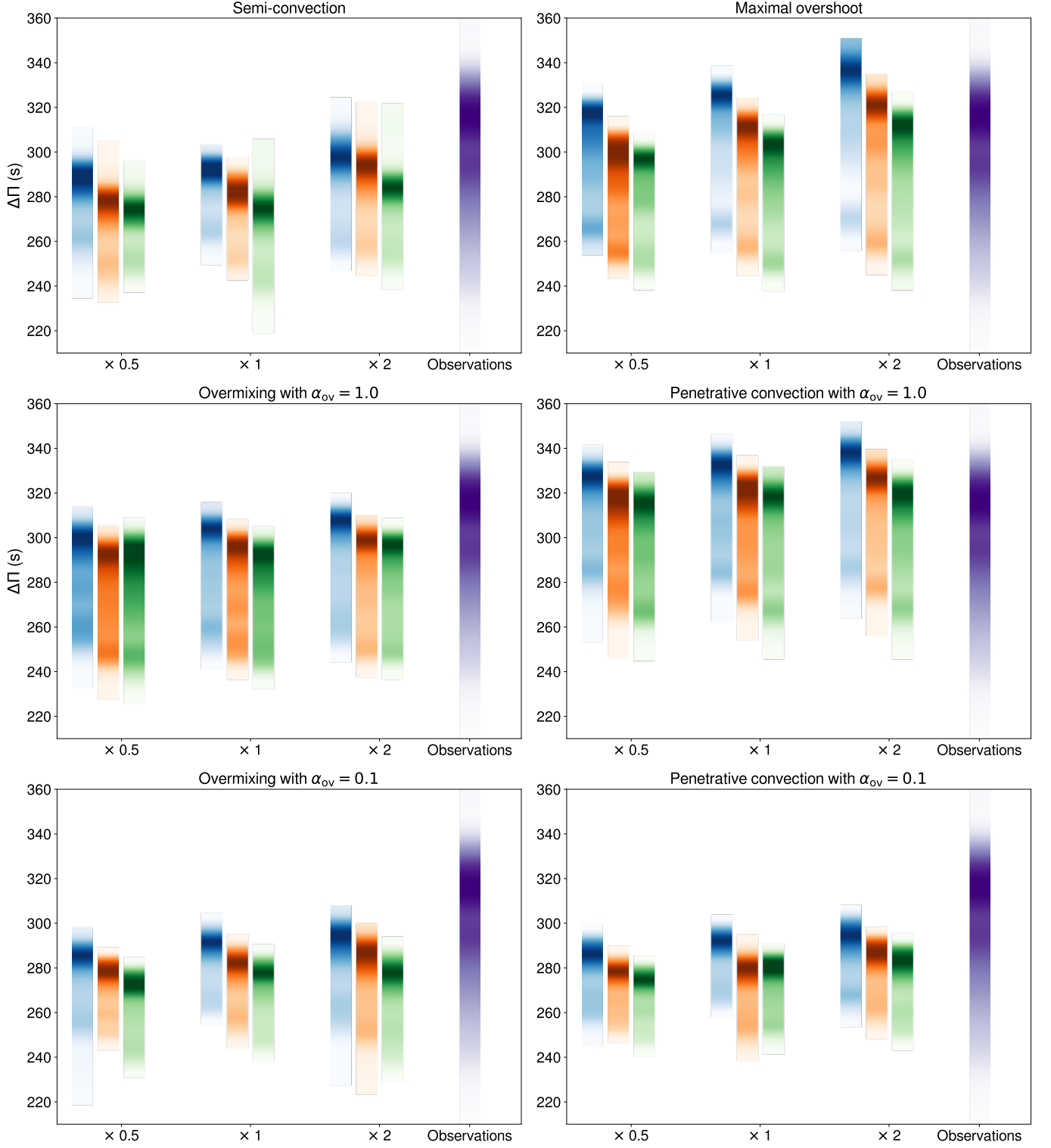


Fig. 9. $\Delta\Pi$ range for models computed with different mixing prescription, $^{12}\text{C}(\alpha, \gamma)^{16}\text{O}$ nuclear reaction rates and metallicities. Models with metallicities of -0.5, 0 and 0.2 dex are shown in shades of blue, orange and green, respectively. The opacity of the bar scales with the time that the model spends at that given value of period spacing. The observations from [Vrard et al. \(2016\)](#) are shown in purple, with the opacity being related to the number of stars observed at that value of $\Delta\Pi$. The models with semiconvection, overmixing and penetrative convection are computed with the CPM scheme.

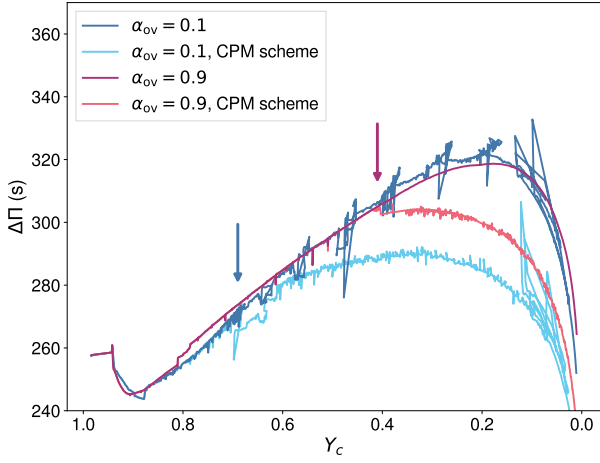


Fig. 10. Evolution of the asymptotic period spacing for overmixing models with $\alpha_{ov} = 0.1$ (blue) and $\alpha_{ov} = 0.9$ (pink), computed with the default core boundary scheme (solid) and the CPM scheme (dashed) (see text for details). The arrows indicate the moment in the evolution from which a semiconvective region appears. Note the strong episodes of core breathing pulses (CBP) in the low overshoot models, for $\gamma_c < 0.15$.

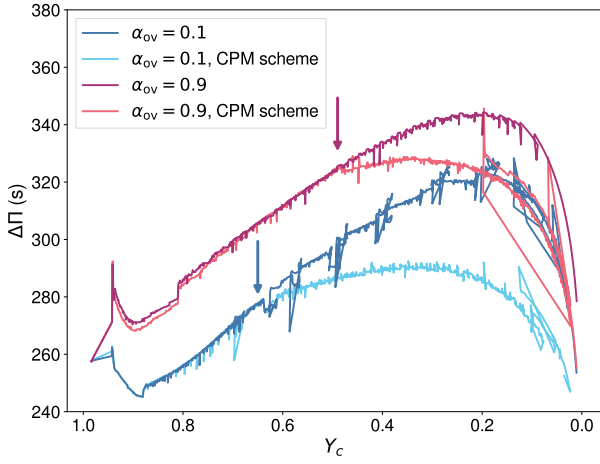


Fig. 11. Same as Fig. 10, now with penetrative convection ($\nabla = \nabla_{ad}$ in the overshoot region.) Similarly to Fig. 10, several CBP events are present.